Environmental Science Nano

ROYAL SOCIETY OF CHEMISTRY

PAPER

View Article Online
View Journal | View Issue

Cite this: *Environ. Sci.: Nano*, 2024, **11**, 911

Nanoplastics prepared with uniformly distributed metal-tags: a novel approach to quantify size distribution and particle number concentration of polydisperse nanoplastics by single particle ICP-MS†

Casey Smith, ‡[a] Stephanie Brown,‡[a] Nathan Malone,‡[a] Shaun Bevers,[b] James Ranville [b] and D. Howard Fairbrother *[a]

Received 29th May 2023,
Accepted 19th December 2023

DOI: 10.1039/d3en00342f

rsc.li/es-nano

Nanoplastics (NPs, <1 μm), the smallest size fraction of environmental microplastics, are a contaminant of emerging concern due their high environmental concentrations, enhanced environmental mobility, and greater bioavailability compared to microplastics. Due to their majority carbon composition, diversity in size, polymer type, surface properties, and shape, NPs are difficult to detect and quantify, hindering our ability to understand NP behavior. To overcome this challenge, we have created irregularly shaped metal-tagged NPs with continuous sub-micron size distributions by cryo-milling lab-generated plastics containing 1% w/w concentrations of an organometallic additive. These metal-tagged NPs are detectable by single particle ICP-MS (spICP-MS) which is capable of measuring NP size distributions (PSD) and particle numbers (PNC) at low μg L^{-1} concentrations. The ease of synthesis and flexibility of this method has enabled a suite of metal-tagged NPs to be created for a range of commercially important polymers (PS, PMMA, PVC, LDPE, PVP). By using unique metal additive-polymer combinations (*e.g.* PS tagged with Sn, PMMA tagged with Ta) the influence of polymer composition on NP environmental behavior can be studied using NP mixtures. Due to the sensitivity of the spICP-MS, we are able to use low metal-loadings to ensure the NPs surface properties remain unchanged compared to unmodified NPs. Advantages of this approach compared to existing NP labelling approaches are discussed along with illustrative examples in laboratory-based studies of NP production from macroscopic plastics (*e.g.* abrasion), photochemical NP degradation, and NP uptake into biological organisms.

Environmental significance

Chemical (*e.g.* photolysis) or physical (*e.g.* abrasion) processes degrade discarded plastics over time into vast numbers of nanoplastics (NPs). Despite a dominance by number and likely importance in determining environmental impacts of plastics, significant analytical challenges have prevented detection and quantification of NPs. We have created metal-tagged NPs with irregular shapes, diverse sizes, and multiple polymer compositions. We demonstrate measurement of particle number concentration (PNC) and particle size distribution (PSD) in complex, heterogeneous matrices at low μg L^{-1} concentrations. This new methodology will facilitate lab-based studies designed to elucidate the behavior and impact of these NPs in aquatic and terrestrial environments as well as the PNC and PSD of NPs released from polymers during chemical and physical processes.

Introduction

Since the 1950s, the production and accumulation of plastics has dramatically increased but only 21% of the cumulative 6500 million metric tons produced by 2015 has been recycled or incinerated.[1] Due to the minimal chemical and biological degradation of most polymers, the remaining portion of plastics has accumulated in landfills or natural environments and generated an estimated 3 million metric tons of microplastics (MPs).[2] In the past decade, public concern has shifted from macroscopic plastic debris to these MPs,[3] typically defined as <5 mm in diameter.[4–8] The observation of MPs in various marine organisms in coastal sediment, soil environments, and drinking water sources such as freshwater

[a] *Department of Chemistry, Johns Hopkins University, Baltimore, MD 21218, USA. E-mail: howardf@jhu.edu*
[b] *Department of Chemistry, Colorado School of Mines, Golden, CO 80401, USA*
† Electronic supplementary information (ESI) available. See DOI: https://doi.org/10.1039/d3en00342f
‡ C. S., S. B., and N. M. contributed equally to this work.

lakes, rivers, and reservoirs[9–11] confirms ingestion as a key route of MP exposure in multiple ecosystems. Additionally, if ingested MPs are transferred from prey to predators, there is a risk for further accumulation at higher trophic levels.[12] This could be an issue for human health if MP accumulation occurs in marine species consumed by humans.[13–16] The uptake of MPs by edible plants is also a public health and food security issue,[17] and consumption of MPs through ingestion of particle-containing food has been cited as a threat to global food security and human health.

MPs that enter the environment originate from two sources: primary or secondary MPs. Primary MPs are plastics intentionally designed with microscale sizes, such as microbeads in cosmetics or microfibers from textiles. Secondary MPs are derived from larger plastic products (*e.g.* fishing nets, containers, *etc.*) that progressively fragment into smaller particles due to natural weathering processes, including photochemical, physical, and biological degradation.[18–21] Given the variety of possible ways in which they can be produced, MPs exhibit heterogeneous morphology, chemical composition, and size.

The fraction of MPs with the smallest sizes (<1 μm) can be separately classified as nanoplastics (NP). Much of the recent literature has used micro(nano)plastics (MnP) to combine both size classes, but this terminology does not acknowledge their very different size regimes and behaviors.[22] *Herein, when specifically discussing plastics with sizes < 1 μm we will utilize the term NP.* A focus on NP behavior is warranted because health hazards will likely be greater for NPs because decreasing size results in an increasing surface-area-to-volume ratio, potential for transport, and facilitated-transport of sorbed contaminants in marine environments.[23–25] Moreover, for the polydisperse particles present in the environment, particle number concentrations increase exponentially as particle size decreases.[26] Consequently, organism exposure is greater for smaller NPs compared to MPs.[27] If uptake occurs, NPs have also been shown capable of eliciting persistent immune and oxidative stress responses that can lead to physiological changes such chronic inflammation and tissue damage.[28–33] Moreover, in drinking water treatment, because particle removal rates generally decrease with decreasing particle size, smaller sized MPs and NPs are of more concern for public health.[34–36] With plastic production estimated to increase 5-fold by 2050[1] and growing evidence of the detrimental health impacts of NPs, developing a fundamental understanding of the behavior and properties of NPs is therefore imperative.

One significant obstacle in studying NP behavior in natural environments is the inherent challenge in their collection, detection, and quantification. Primary difficulties include obtaining a sufficient number of NPs to allow analysis and distinguishing these plastic particles from naturally occurring, carbon-based particles (*e.g.* cells, detritus). In principle, NPs could be fractionated and concentrated separately from background particles by means such as density separation, sieving, and selective digestion of sediment particles with peroxide. However, these preparatory steps can influence the final size and surface properties of the NPs.[37,38] Incomplete removal of extraneous material results in the presence of background particles in the sub-micron size range, which leads to an overestimate of NPs in the sample.[37] A few high resolution separation techniques (*e.g.* field flow fractionation) are capable of discriminating NPs from some natural environmental constituents (*e.g.* NOM), although these methods have yet to find widespread implementation.[39,40]

Even if NPs can be successfully separated from interfering natural particles, identifying their chemical composition, determining their physicochemical properties (*e.g.* size), and quantifying their concentration, are acutely difficult for all but the most pristine samples.[41,42] Laser-based sizing techniques, such as dynamic light scattering (DLS), can measure NP particle size distribution (PSD) but not concentration (PNC, # of particles per mL), and nanoparticle tracking analysis (NTA), which can provide both PSD and PNC, is limited to sub-micron sizes. The inability of NTA and DLS to differentiate NPs from background particles also prevents their use for most environmental matrices.[43,44] In principle PSD and PNC of NPs is possible by using single particle ICP-MS (spICP-MS) analysis using ^{13}C.[45] This less abundant isotope of carbon (1.16%) is used to avoid the high natural ^{12}C background ICP-MS signal generated by the ubiquitous presence of carbon dioxide. However, the high ionization potential of carbon (11.26 eV), which causes a low (<5%) ionization efficiency in the plasma, combined with high carbon background functionally limits ^{13}C spICP-MS analysis to sizes above 1.5–2 micron for PS.[45] Furthermore, the use of ^{13}C for NP quantification in complex environmental samples where carbon-containing particles are present is not possible. Electron microscopy (EM) techniques such as scanning electron microscopy (SEM) and transmission electron microscopy (TEM) are capable of measuring PSDs at micro- and nanoscale dimensions, respectively, but similarly cannot easily distinguish NPs from other carbon-based particles. With EM, there is also great difficulty translating the particle numbers observed in each image to the aqueous PNC in the original sample.[46] EM is also a low-throughput technique and drying effects during sample preparation may cause unwanted particle aggregation leading to PSD distortion.

The numerous issues associated with the collection, detection, and quantification of NPs in the natural environment provide the impetus to generate NPs specifically for the purpose of laboratory-based studies. Researchers often use readily available, commercially synthesized materials to study NP behavior,[47] but with several drawbacks. For example, the surfaces are often modified with surfactants to facilitate dispersion and the NPs are produced as monodisperse spheres. This makes commercially synthesized NPs a poor proxy for the irregularly shaped and polydisperse NPs found in natural environments. Furthermore, the range of polymers commercially available as NPs is extremely limited (typically only polystyrene and poly(methyl methacrylate)). The alternative for researchers is to create NPs in house. NPs can be synthesized bottom-up *via* polymerization,[48–51] but the synthesis process limits their resultant heterogeneity in polymer type,

size, shape, and surface morphology.[47] In contrast, NPs can be created top-down from bulk polymers through laboratory weathering, accomplished through a combination of UV exposure and mechanical abrasion,[52] sonication-based fragmentation,[53,54] or from cryogenic milling.[55,56] A key advantage of these top-down methods is the ability to recreate the heterogeneity in size, shape, and surface morphology of NPs generated from plastic waste under environmental conditions.[57] However, without the inclusion of a tracer, these NPs cannot be sized, quantified, or tracked in complex, realistic environmental matrices. This is due primarily to the inability of most analysis methods to differentiate NPs from other carbon-containing "background" particles, clays and other naturally occurring submicron particles, which are likely present at much higher concentrations. This severely limits the use of model NPs in laboratory studies designed to study their environmental behavior (*e.g.* biological uptake or transport studies).

To overcome these issues, NPs modified by the addition of identifiable tracers, specifically fluorophores or metals, have been synthesized and employed.[38,58–60] These labelling approaches render the NPs distinguishable from other background particles with use of an appropriate analytical technique.[61,62] The use of fluorophores is, however, generally used to quantitatively determine NP uptake or track their movements using techniques such as imaging by fluorescence microscopy.[38,63,64] In contrast, the analysis of metal tagged NPs by ICP-MS provides quantitative NP mass concentrations but no information on PSD or PNC.

In this paper, we present a new labelling approach which involves the top-down synthesis of irregularly-shaped, polydisperse NPs which contain uniform concentrations of embedded (*i.e.* tagged) organometallic additives. Incorporating organometallic compounds at a low loading (1% w/w) does not alter the bulk or surface properties of the NPs and enables spICP-MS measurement to determine PNC and PSD for a range of commercially important NPs (including PS, PMMA, PVC, LDPE, PVP) in complex matrices. Cryomilling creates NPs whose PSDs span the full submicron range, with the greatest number occurring at the very smallest sizes. This new methodology can be easily implemented in different research laboratories having ICP-MS capabilities. Furthermore, we provide several example environmental applications to demonstrate suitability of the approach to NP analysis.

Materials and methods

Selection of plastics and organometallic additives

Given the broad range of polymers used to manufacture plastics, we demonstrated the general utility of our approach by preparing metal-tagged NPs using five commercially available polymers with varying chemical characteristics. These polymers have also been previously detected as MPs in relatively high quantities in a range of natural environments.[65–67] (1) Polystyrene (PS) a hydrophobic polymer, found in packaging, containers, lids, bottles and trays; (2) low density polyethylene (LDPE), a hydrophobic plastic used to make containers, plastic bottle tops and packaging; (3) polyvinyl chloride (PVC), used to make pipes, non-food packaging, and plastic cards; (4) polymethyl methacrylate (PMMA), a hydrophilic polymer used in cell phone screens and as a substitute for glass in lenses; (5) polyvinylpyrrolidone (PVP), a hydrophilic polymer which, along with LDPE and PMMA, has been used as plastic microbeads in cosmetics. Organometallic complexes were selected as the metal-tag source (*e.g.* Ta, Sn, and Zr) based on the following criteria: (i) solubility in a volatile organic solvent also capable of dissolving the selected polymer, (ii) the metal's sensitivity for detection by spICP-MS, and (iii) the metal's low abundance in the environment, thereby facilitating discrimination of the metal-tagged NPs from background signals (*e.g.* clays containing metals such as Al, Fe, Si, Ti).

All chemicals were used as received without further purification. All organic solvents used were ACS reagent grade. Poly(methyl methacrylate) (MW = 168 000), polystyrene (MW = 280 000), polyvinylchloride (MW = 35 000), polyvinylpyrrolidone (MW = 10 000), and low-density polyethylene (MW = 4000) were purchased from Sigma Aldrich. Organometallic complexes tantalum(v) ethoxide, tantalum(v) chloride, zirconium(iv) ethoxide, and platinum 2,4-pentanedionate were purchased from Alfa Aesar. Dibutyltin diacetate was purchased from TCI Chemicals.

Synthesis of metal-tagged plastics

Metal tags were incorporated into each of the polymers *via* solution blending[68,69] where mixture of organometallic additive and polymer are sonicated in an organic co-solvent. Solution blending was preferred over melt mixing/extrusion to optimize uniformity of additive dispersion within the polymer, an important attribute in determining NP size distribution.[70,71] All % w/w values herein refer to the mass loading of organometallic additive with respect to mass of polymer. Unless otherwise noted, a 1% w/w additive loading was used to create the casting solution. Once both additive and polymer were visibly dissolved, the blended solution was poured into an aluminum dish (12.7 cm, Juvale, Amazon), and the solvent subsequently volatilized at room temperature for approximately 48 hours (Fig. S1†). To ensure full solvent removal from the material, the composite was dried under vacuum at 35 °C for an additional 48 hours. All composites were then recovered from the aluminum dishes and trimmed to a uniform size, approximately 9 cm diameter. The mass of polymer and metal additive used are gravimetrically determined during synthesis. Given that the polymers and the additives are involatile and there is no material loss during solution blending except for solvent evaporation, the metal content in the polymers can be assumed to be well determined.

A schematic of the solution blending process demonstrating the preparation of PS containing Sn and PMMA containing Ta using chloroform and benzene, respectively, as co-solvents is shown in Fig. 1. Table 1 describes the organometallic additive, polymer, and solvent combinations utilized to create metal-

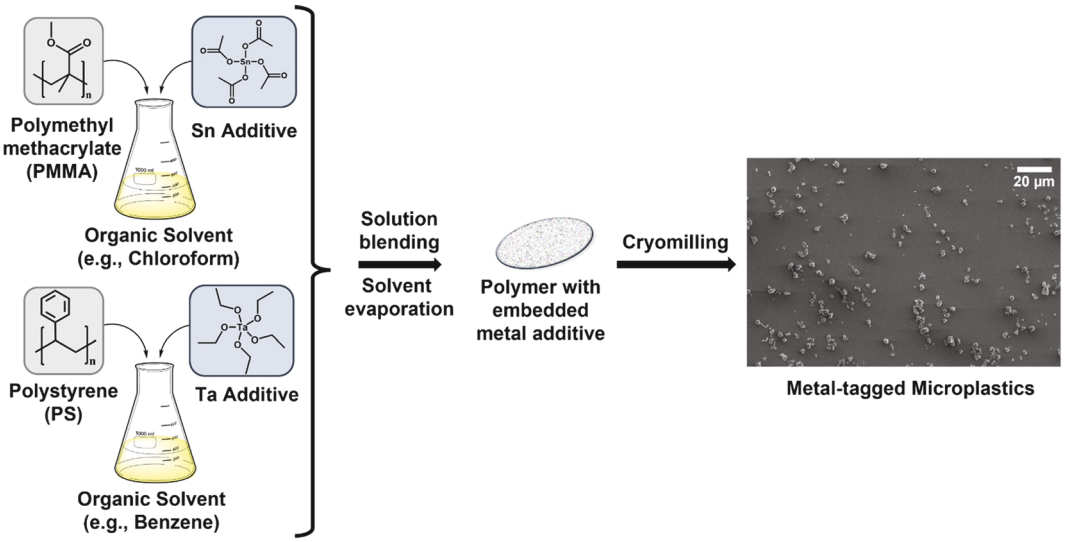

Fig. 1 Synthesis of nanoplastics (NPs) with embedded metal tags. The metal tags are incorporated into the polymer by solution blending before NPs are generated by cryomilling. The SEM image shows an example of colloidally stable NPs produced in this way (see text for details).

tagged NPs to-date. Further detail regarding each composite synthesis (reagent masses, solvent volume, and sonication time) can be found in Table S1.†

Generation and characterization of metal-tagged nanoplastics

Metal-tagged composites were cut into approximately 1 × 1 cm^2 pieces for milling in polycarbonate cryomill tubes with a stainless-steel impactor and end caps (Spex 6700 Freezer/Mill). Composites were cooled with liquid nitrogen and milled for a total of 30 minutes (6, 5 minute cycles) at an impact frequency of 15 Hz with a 2 minute cool period between cycles. This process served as an accelerated form of mechanical erosion/fracturing and generated irregularly shaped NPs that contained a broad range of particle sizes, from nanometer to micron (Fig. 1).

The physiochemical properties of the metal-tagged plastics were determined using a combination of attenuated total reflectance-infrared spectroscopy (ATR-IR), differential scanning calorimetry (DSC), water contact angle measurement, and X-ray photoelectron spectroscopy (XPS). All data were acquired on the cryomilled powders, except for the water contact angle measurements which used the as-prepared composites. Additionally, μ-X-ray fluorescence (μ-XRF) mapping of the metal-tagged plastics (M4 TORNADO μ-XRF (Bruker)) was used to determine the distribution of metal additive within the plastic composites. Further details on data collection and analysis are provided in the ESI.†

Preparation of water-stable nanoplastic suspensions

Cryomilled plastic particles were added to deionized water at a concentration of 1 mg mL^{-1} and sonicated in an ice water bath (Branson 1510 ultrasonicator bath, Danbury, CT) for 24 hours. After sonication, the solution was allowed to settle undisturbed for another 24 hours in an Erlenmeyer flask. The supernatant was then removed from approx. 0.5 cm below the surface to approx. 0.5 cm above the bottom of the flask to collect only those particles that remained in suspension. The degree to which different NPs formed stable suspensions depended on

Table 1 Combinations of organometallic additive, polymer, and solvent utilized to create metal-tagged NPs to-date. A "check" indicates successful yield of homogenous composite. An "✗" indicates a failed composite

	Tantalum(v) ethoxide	Dibutyltin diacetate	Zirconium(iv) ethoxide	Platinum 2,4-pentanedionate	Tantalum(v) chloride
	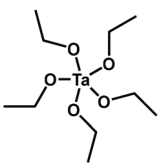	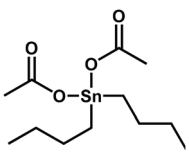	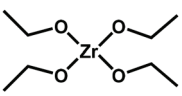	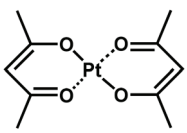	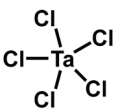
PS	✓ benzene or THF	✓ THF	✓ benzene	✗ chloroform or THF	✗ chloroform
PMMA	✓ toluene or THF	✓ THF	✗ toluene	✗ toluene	✗ chloroform
PVP	✓ methanol				
PE	✓ toluene				
PVC	✓ THF	✗ THF			

the polymer type. To determine suspension efficiency, a known volume of the isolated supernatant was lyophilized and mass of suspended microplastics measured. 100% of PVP, a water-soluble polymer formed stable colloidal NPs at a mass loading of 1 mg mL^{-1}. For the other polymers tested, lower fractions of the initial 1 mg mL^{-1} suspension remained stable. Specifically, suspension efficiencies for PMMA, LDPE, and PS were 13.7%, 8.8%, and 5.9%, broadly in line with their respective hydrophilicities.[72]

Quantification and sizing of metal-tagged nanoplastics

Single particle optical sensing analysis (SPOS) (Particle Sizing Systems – SNS 760) was used to characterize the number and size distribution of NPs in the size range of 0.5–500 μm. The SPOS software combined the data from an extinction sensor (180° angle) and a scattering sensor (135° angle). Additionally, SEM (JEOL, JSM-IT100) was used to assess the surface morphology and size of nanoplastics.

The principal method used for size characterization of the metal-tagged nanoplastics was spICP-MS (Perkin Elmer NexION 300 D) analysis of water-stable NP suspensions. As discussed in the introduction, spICP-MS is uniquely well suited to quantify PSDs and PNCs of metal-tagged NPs (schematic workflow is shown in Fig. 2). NPs were analyzed for ^{181}Ta, ^{118}Sn, and ^{90}Zr. Suspensions were introduced into the plasma using a Meinhard nebulizer (ESI, Golden CO) and a cyclonic spray chamber (PerkinElmer, Waltham, MA). Each time a metal-tagged NP enters the ICP plasma it is vaporized, generating a discrete plume of metal ions that are mass-selected by a quadrupole and registered as a pulse in the detector's time resolved output. These particle generated pulses are registered when the signal exceeds a threshold value,[73] which is typically set as the mean of all background signals plus three times the standard deviation ($\mu + 3\sigma$). In a 60 second analysis using 100 μs dwell times, it is typical to measure on the order of 1000–10 000 particles. The size-based method[74] was used to determine transport efficiency (TE), which ranged from 5–8% throughout the study.

After accounting for TE, NPs can be sized and counted using the metal mass detected in each individual NP. Assuming a uniform distribution of metals in the plastic, the intensity of each pulse measures the NP effective size/diameter through:

$$\text{NP Volume } (V) = \text{Sum of Pulse Intensities} \times \frac{\text{Metal Mass}}{\text{Intensity}} \times \frac{\text{NP Mass}}{\text{Metal Mass}} \times \frac{1}{\text{Polymer Density}}$$

The effective spherical NP diameter (d) can then be determined from:

$$V = \left(\frac{\pi d^3}{6}\right)$$

A notable advantage of spICP-MS is its extreme sensitivity. Each NP contributes only a small amount of mass (femtograms) to the suspension. Thus, suspensions of metal-tagged NPs are measurable at part-per-billion mass concentrations. The number of pulses per volume sampled, after accounting for flow rate and TE,[74] provides PNC. It should be noted that although the NPs are not spherical, no particles of high aspect ratio are formed by cryomilling (Fig. 1), thus computation of an equivalent spherical diameter from the spICP-MS analysis does not introduce significant error. Furthermore, as a consequence of the cubic relationship between mass (volume) and size there is a relative insensitivity of the PSD to small uncertainties in the mass loading of the metal.

To evaluate the ability of spICP-MS to simultaneously discriminate different NPs prepared with different metal tags in a mixture, a suspension containing NPs of PS loaded with zirconium(IV) ethoxide, PMMA loaded with dibutyltin diacetate, and PVP loaded with tantalum(V) ethoxide was prepared. To achieve equal amounts (by number density) of the three plastics in suspension, the initial mixture contained 16.5% PMMA, 0.04% PVP, and 83.4% PS by mass. This was necessary to account for the different hydrophobicities of the three polymers.

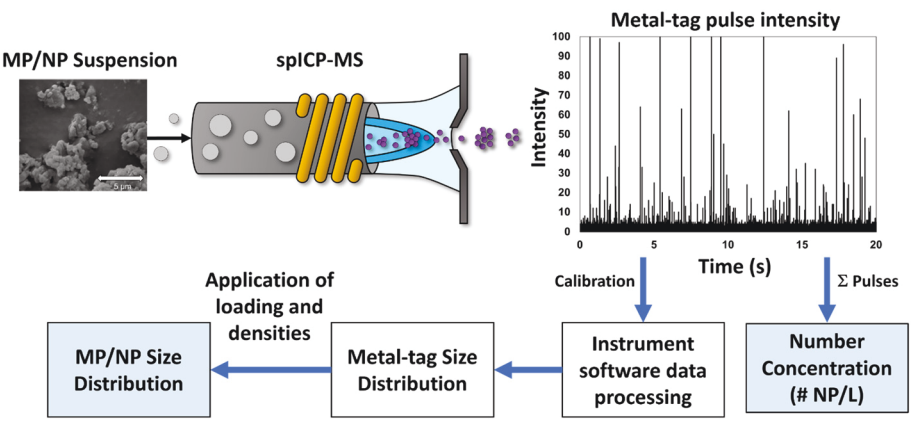

Fig. 2 Single-particle ICP-MS quantifies the number concentration, mass concentration and size distribution of <1 μm sized metal tagged nanoplastics (NPs).

Applications of metal-tagged plastics and nanoplastics in lab-based studies

To illustrate the benefits of using metal-tagged plastics and nanoplastics in lab-based studies we conducted demonstrative studies across three environmentally relevant scenarios. In each of these experiments PNC and PSD were determined *via* spICP-MS.

Abrasion. A PMMA composite loaded with 1% w/w dibutyltin dilaurate was abraded with 320 grit sandpaper and particulates formed suspended in DI water.

Photolysis. A solution of PMMA NPs containing 1% w/w tantalum(v) ethoxide was irradiated at 300 nm in the presence of 200 mM H_2O_2 for 0, 3, 6, and 12 hours. Additional experimental details are provided in the ESI.†

Biological uptake. Developing zebrafish larvae were exposed to suspensions of heterogeneously sized PMMA NPs and tissues collected for metal analysis. Further experimental details are provided in the ESI.†

Results and discussion

Characterization of metal-tagged plastics and nanoplastics (NPs)

We utilized a combination of ATR-IR, DSC, water contact angle, and XPS to ensure that the physiochemical properties of the metal-tagged polymers remain unchanged from the native polymers. ATR-IR assessed the extent to which the addition of the metal tags caused any observable changes in the chemical bonding. There were no observable differences in ATR-IR data for plastics with and without the presence of 1% w/w organometallic additive (Fig. S2†). Similarly, DSC was used to compare the thermal properties of the polymers after introduction of metal tags. Analogous to the ATR-IR data, Fig. S3–S5† indicated no change to the thermal transitions of the plastics with incorporation of 1% w/w organometallic additive.

Surface chemistry and surface properties are key to determining adsorption, interparticle interactions, and colloidal transport.[75–83] Water contact angle measurements provided a quantitative metric to assess the relative surface hydrophilicity/hydrophobicity of each plastic.[84,85] As demonstrated in Table S2,† there were no significant differences in the measured water contact angle for plastics prepared with and without 1% w/w organometallic additive. To further probe the surface properties of the metal-tagged NPs, XPS was used to examine the elemental composition and bonding state of the surface atoms. As demonstrated in Fig. S6–S9,† the elemental composition and bonding state of the plastic surface remains unchanged by addition of 1% w/w organometallic additives, irrespective of the polymer or the metal additive. Moreover, analysis of the principal metal transitions for each additive (*e.g.* Ta(4f) for Ta(v) ethoxide) indicated that the metal atom concentration at the surface is below the XPS detection limit (approximately 0.1 at%), consistent with expectations. For example, in the case of PS containing 1% w/w Ta(v) ethoxide the calculated at% Ta is approx. 2.6×10^{-4}. These results strongly indicate that the physical and chemical properties of the plastic surface remain unaffected by the introduction of the metal-tags. Therefore, it is reasonable to assume that the interfacial properties of the metal-tagged NPs will be a mirror of the unmodified NPs.

NP sizing using spICP-MS relies on metal additives being distributed relatively uniformly within the composite. μ-X-ray fluorescence (μ-XRF) mapping of the metal-tagged plastics was used to determine the distribution of metal additive within the polymer matrix. Whereas 1% w/w $Sn(C_4H_9)_2(C_2H_3O_2)_2$ PS (Fig. 3) and other organometallic complexes produced reasonably uniformly dispersed metal-tags (Fig. S10 and S12–S17†), the inorganic salt, $TaCl_5$, was distributed heterogeneously in the composite (Fig. S11†), likely a

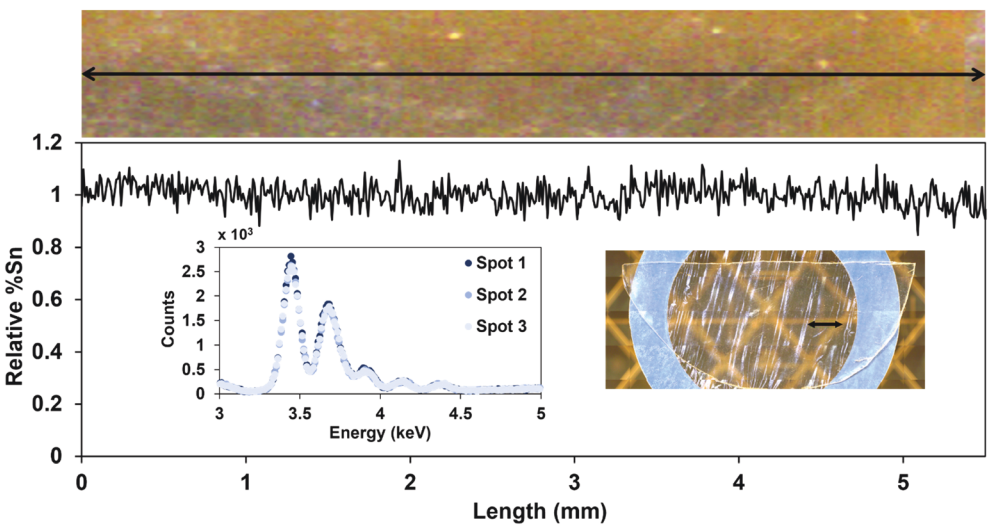

Fig. 3 μ-XRF of a 1 w/w % Sn-PS composite. Shown is the relative % Sn detected as a function of composite length to demonstrate the uniformity of metal loading within the plastic. Data collected at a 10 μm spot size over a sample distance of 5 mm.

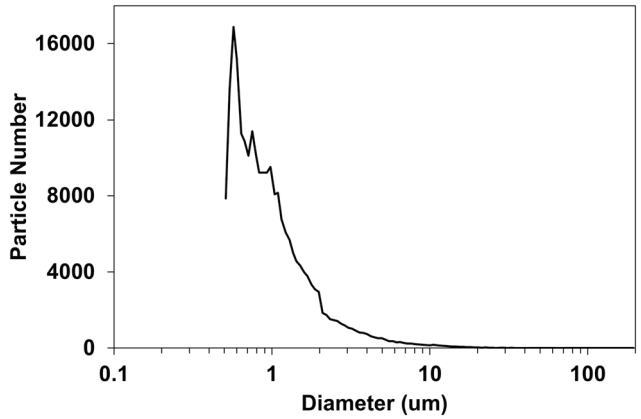

Fig. 4 Particle size and number distribution determined by SPOS for a 1 w/w % Sn-PS NP suspension.

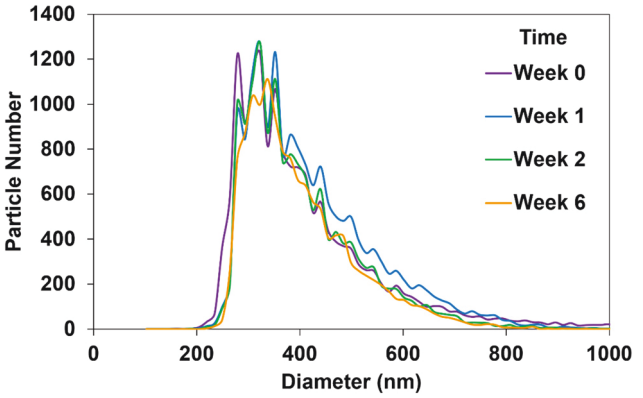

Fig. 5 Particle size distribution determined by spICP-MS for a 1 w/w % Ta-PMMA suspension stored in the dark at room temperature and sampled over 6 weeks.

consequence of poor dispersion in the PS matrix. This extremely non-uniform dispersion means that the mass of Ta in a given volume of PS will be inconsistent and lead to inaccurate measurement of particle size *via* spICP-MS. Our results suggest that organometallic precursors with alkyl ligands are better suited than inorganic ligands (*i.e.* salts) to produce uniform dispersions of metal tags in the majority of polymers.

Quantification and sizing of metal-tagged nanoplastics

Single particle optical sensing analysis (SPOS) (Particle Sizing Systems – SNS 760) was used to characterize the number and size distribution of colloidal Sn-tagged PS NPs (Fig. 4). Particle numbers rapidly increase with decreasing size, increasing the probability that submicron particles are undercounted and oversized due to multiple particles being present in the measuring volume (*i.e.* coincidence). SPOS analysis shows that 96% of the MPs are less than 5 μm and 60% are less than 2 μm in size, although there is a clear instrumental size cut-off for NPs below 700 nm. This size limitation and lack of particle specificity (all particles generate a signal regardless of composition) means that SPOS cannot be used to determine NP number concentrations or size distributions in samples that contain NP mixtures or heterogeneous samples that contain other types of particles (*e.g.* water samples containing background natural mineral particles).

As seen in Fig. 5, the size distribution of 1% w/w $Ta(OC_2H_5)_3$ PMMA NPs are observed at sizes between 200 and 700 nm with an exponential increase in particle number with decreasing size. This distribution has been commonly observed for natural particles[86] and we propose will also reflect the PSD of NPs generated by the environmental weathering of plastic waste. The effect on spICP-MS analysis of rapidly increasing particle number with decreasing size has been thoroughly explored in a companion study.[87] Although we have not explicitly explored this aspect, other studies have also shown that the PSD of NPs produced from polymers can be tuned by varying the conditions of the cryomilling process (*i.e.* frequency, number, and duration of cycles).[88–91] A potential analytical artifact of our metal-tag approach is the leaching of metal additive from the plastic over time when in aqueous suspension, which would manifest itself as a particle size distribution and particle number count that decreased over time. However, additive leaching rates from plastics are extremely low.[92–95] Consistent with this concept, we have experimentally verified that the NP number concentration and size-distribution of these Ta-PMMA NPs remains stable in water over the course of six weeks (Fig. 5). Given this observation, there is no reduction to the metal loading in the NP that would indicate measurable additive leaching over this timescale.

There is a lower size limit of metal-tagged NPs that can be detected by spICP-MS as seen in Fig. 5 and 6. The existence of this limit can be understood by recognizing that in spICP-MS each NP is detected as a metal pulse and the sum of these pulse readings is proportional to the mass of metal in the NP. The lower limit for NP detection is determined by the smallest individual signal associated with a metal-tagged NP that can be distinguished from the background signal (see Fig. 2). Thus, for NPs below a certain size, the metal pulse generated in the spICP-MS will be too small to be discriminated from the background. Undercounting of particle numbers near the background can arise due to multiple factors.[96] The mode, which lies above the limit established by sensitivity (vertical lines in Fig. 6) can be considered a "practical" lower limit for quantifying the PSD of the NPs. As the metal loading increases, this "practical" lower limit will decrease, as we observe with the modal size for Ta-PVP quantification decreasing from 0.31 to 0.17 μm as the Ta loading increases from 0.1 w/w% to 1 w/w% (Fig. 6). It should be noted that increasing the metal loading from 0.1 to 1% only decreases the minimum detectable particle size by a factor of 2.15 due to the cubed relationship between diameter and volume. Similarly, if we were to decrease the threshold size by another factor of approx. 2 this would require increasing the metal loading to 10% with an increasing likelihood that some NP physicochemical (*e.g.* surface) properties will differ from those of the pristine NPs.

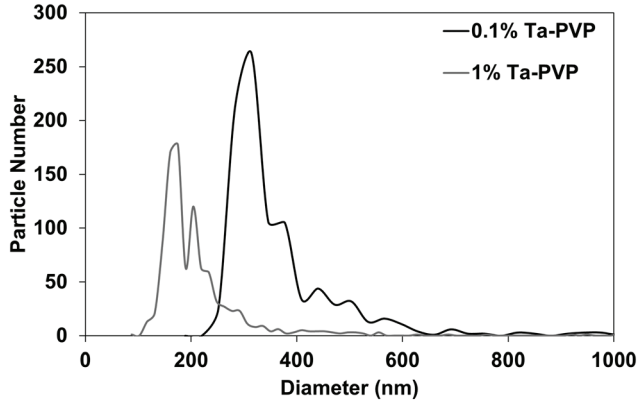

Fig. 6 Particle size distributions of 0.1 w/w % Ta-PVP and 1 w/w % Ta-PVP NP suspensions. The minimum NP size measured by spICP-MS is directly affected by the organometallic additive weight % loading.

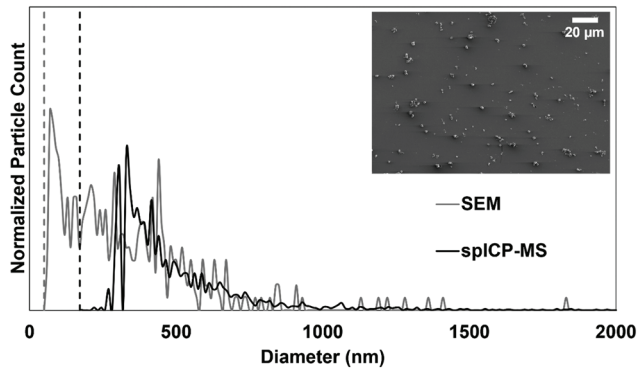

Fig. 7 Illustrative comparison of the particle size distribution determined by SEM *vs.* spICP-MS for the same colloidal suspension sample of 1 w/w % Ta-PMMA NPs. Counts were normalized by the overlapping area (> = 260 nm diameter); 403 particles were detected by SEM and 3160 by spICP-MS.

The suitability of spICP-MS for sizing NPs is revealed in Fig. 7, where the PSD of Ta-PMMA NPs determined by spICP-MS is compared to that obtained by SEM. Both SEM and spICP-MS reveal that NPs are detected almost exclusively below approximately 1 μm and that PNCs exhibit similar exponential decreases between approximately 0.3–1.0 μm, the former representing the size threshold for spICP-MS detection of these NPs. As expected, SEM analysis reveals that PNCs continue to increase for particles sizes < 0.3 μm. The qualitative agreement in the size distributions measured by spICP-MS and SEM provides strong support for the validity of the steps involved in converting the number concentration of metal pulse areas observed by spICP-MS into the equivalent spherical size distribution.

Alternative NP and MP labelling techniques

Herein we have described a new method to create labelled polydisperse NPs containing uniformly incorporated metal tags. However, it is important to compare this approach to other recently developed methods for tagging NPs. These tags have either been attached to the NP surface, incorporated into the polymer matrix, or involve the synthesis of a "core–shell" structure.

A relatively straightforward labeling approach is staining the NP *via* adsorption of a fluorescent dye, such as Nile red.[37,38] However, some polymers including polycarbonate, polyurethane, polyethylene terephthalate, and polyvinyl chloride, have been shown to fluoresce only weakly after staining with Nile red, limiting its applicability to lower density (and generally more hydrophobic) plastics.[38] Moreover, since the staining is restricted to the NP surface, the fluorophore concentration and thus the fluorescence signal of each particle is limited. The NP surface properties could also be altered by adsorption of the dye. In addition to staining, NPs with embedded fluorescent dyes can be obtained commercially, although these NPs are expensive, typically only obtainable for a limited number of plastics (*e.g.* PS, PMMA), and generally produced as monodisperse spheres rather than the heterogeneous shapes representative of naturally occurring NPs. Moreover, these NPs are often stabilized in solution by surfactant molecules or have chemically modified surfaces which alter their nascent surface properties. The primary advantage of fluorescent labels is in qualitative tracking of NPs, for example in organism bioaccumulation or exposure/toxicology studies.

The alternative to fluorescence as a NP labelling strategy has been to incorporate metal tags in a bottom-up synthesis and rely on ICP-MS (or less frequently spICP-MS) as the basis for detection and quantification. For observing NP distribution in matrices such as tissue, the application of ICP-MS is a rapidly expanding field. For example, laser ablation inductively coupled plasma mass spectrometry (LA-ICP-MS) provides *in situ* elemental mapping,[97,98] but is a relatively new analytical development and has yet to reach the widespread popularity or appeal of fluorescence microscopy. Some of the advantages of metal-tags over fluorescence-based labelling methods, include tag-stability to photochemical weathering, easy quantification, and a broader range of polymer types that can be labeled. One metal-based labelling approach involves attaching the metal probes (nanoparticles, ions, or hydrophobic organometallic compounds) to the surface of the MPs or NPs through physical adsorption or chemical binding, enabling detection of NPs ≤ 2 μm.[58–60] However, the use of surface attachment strategies could alter the NPs interactions and therefore environmental behavior. Additionally, labeling particles with metal ions adsorbed to the NP surface has proven challenging as dilution may cause ions to desorb. More stable attachment occurs when positively-charged metallic nanoparticles are coupled with negatively-charged (carboxylate) functional groups on the NP surface through electrostatic interactions, although this approach will almost certainly impact NP surface properties.[58,59] While most studies utilize ICP-MS to track the mass concentration of metal-tagged NPs, in principle metal-based surface tags can also serve as a means of sizing NPs using

spICP-MS, assuming the amount of tracer present is proportional to the size of the NP. To determine size, both the surface coverage (mass/area) and particle shape must be known and uniform. Validation is difficult for tagging techniques that rely on sorption, as the coverage is usually not quantifiable and desorption of adsorbed tags may occur with changes in concentration, pH, or temperature. Moreover, if some of the metal tags desorb into solution, the size limit for detection by spICP-MS will increase, analogous to an increase in the NP size threshold described in Fig. 6.[60]

A more recent alternative to surface-bound metal tags, has been fabrication of monodisperse NPs with well-defined shapes (usually spherical or sphere like) through the incorporation of metals into the core of the NP, creating a core–shell structure. One of the first metal-tagged NPs generated in this way used a polyacrylonitrile (PAN) core that contained Pd surrounded by a crosslinked polystyrene shell.[99] Since the Pd atoms are localized within the PAN core rather than adsorbed on the surface of the NP, the surface properties of the polymer remain uncompromised and Pd release unlikely. Additionally, Pd exists at low concentrations in the environment, making it an ideal metal tag for NP detection. The mass recovery of these NPs was quantified by conventional ICP-MS after spiking into complex environmental matrices (*e.g.* activated sludge before treatment in pilot-scale batch reactors).[99] Following the initial study, the Pd-containing NPs also found utility in tracking PS NPs in a diverse range of biological and environmental media.[62,100–103] This procedure does, however, requires a complex multi-step synthesis where multiple solvents are added in sequence to a reaction vessel, and has not been extended to polymers other than PS. To date, only mono-dispersed approx. 100 nm NPs with a smooth or "raspberry-like" morphology have been synthesized. Recently a more complex core shell NP was synthesized *via* intercalation of metal chloride salts (Au, Pd, or Pt) into a porous core[104] followed by the reduction of the salts to elemental metal. The metal-imbued core was then coated with either PMMA or PS. Metal intensity distributions obtained by spICP-MS analysis indicated a narrow range of mass loadings in all three NP types, but NP size could not be computed from metal mass as the metal only resided in the core and not the shell. Alternatively, Au nanoparticles have been used as a core and coated with a PS, polyacrylic acid copolymer shell to avoid metal salt reduction.[39] spICP-MS coupled to field flow fractionation was able to determine the Au nanoparticle loading in each polydisperse NP.

Size analysis and measurement of PNC of non-tagged NPs is also possible by spICP-MS analysis using ^{13}C.[45] This less abundant isotope of carbon (1.16%) is used to avoid the high natural ^{12}C background ICP-MS signal generated by the ubiquitous presence of carbon dioxide. The high ionization potential of carbon (11.26 eV), which causes a low (<5%) ionization efficiency in the plasma, combined with high carbon background functionally limits ^{13}C spICP-MS analysis to sizes above 1.5–2 micron for PS.[45] Furthermore, the use of ^{13}C for NP quantification in complex environmental samples where carbon-containing particles are present is not possible.

Advantages and applications of polydisperse NPs with uniformly distributed metal tags

The new NP labelling method described herein has a number of advantages compared to existing labelling strategies. For example, this synthetic strategy uses readily available, cheap, pre-synthesized polymers and organometallics as compared to bottom-up polymerization techniques.[99] The solution blending required to generate the metal-tagged plastics is straightforward to implement, making it ideally suited to widespread adoption within different research labs. The method can also be applied to a broad range of polymers which have been detected as NPs in the environment. Specifically, three of the polymers (PE, PS, and PVC) included in our syntheses described in Table 1 account for over 50% of all non-fiber plastics produced.[1] Moreover, the choice of polymer is not limited by its thermal properties, and only requires consideration of polymer and metal-tag solubility when selecting a volatile, organic solvent for preparing composites. Therefore, this method could be extended to metal-tag numerous other natural or synthetic polymers.

For the metal-tagged NPs synthesized by this new method, the entire volume of the NP is used for detection in contrast to other labelling techniques that rely on adsorption,[60] direct attachment,[58–60] or the presence of metal atoms on the NP surface. Because of this distribution, the metal additives are present at higher concentrations per NP than other labeling methods and yet maintain undetectable surface concentrations. For example, in a 1 μm sized spherical particle, over 99% of the metal-tags are more than 1 nm from the surface. As a result, the majority of metal atoms contributing to the spICP-MS signal are contained within the bulk of NP where they do not impact surface properties. This is confirmed by the absence of any difference between water contact angle or ATR-IR spectra observed between metal-tagged and pristine (unmodified) polymers. Since NPs are typically non-porous, PSDs generated by spICP-MS can also estimate geometric surface areas, information that is otherwise extremely difficult to obtain.

To illustrate the range of environmental studies where plastics and polydisperse NPs with uniformly distributed metal-tags can be used effectively we have conducted a number of simple studies. For example, the uniform distribution of the metal-tags throughout the plastics and NPs enables determination of size-dependent concentrations of NPs produced in various transformation processes *via* spICP-MS, a capability which does not exist for metal core–polymer shell NPs. To demonstrate this ability, we measured the PSDs of NPs generated by physical abrasion of a macroscopic plastic sample. spICP-MS analysis revealed that the abrasion process produced NPs in the 0.3 to 1 um size range (Fig. 8), an approach that could be expanded to quantify both the efficiency and PSD of NPs generated from different polymers under more well controlled abrasion conditions. In this application our synthetic procedure also enables selection of specific metal-tags, notably

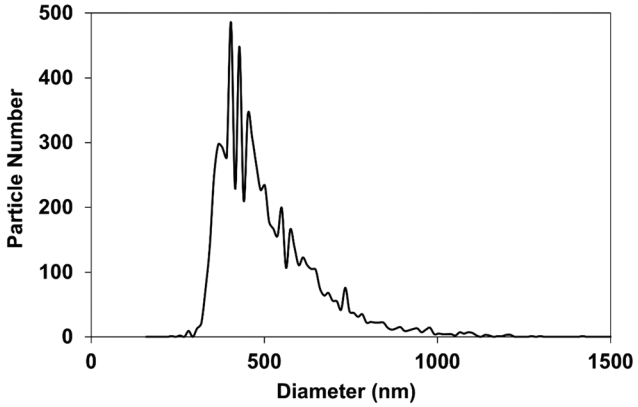

Fig. 8 Particle size distribution of 1 w/w % Sn-PMMA NPs generated by physical abrasion of a macroscopic 1 w/w % Sn-PMMA sample.

metals (*e.g.* Ta, Sn) that not only exhibit high sensitivity in the spICP-MS but are also absent in most environmental matrices. In the context of abrasion studies for example this allows us to discriminate NPs produced from the polymer from natural NPs present in the natural environment or those produced by the abrading material.

spICP-MS can also follow the size dependent evolution of NPs in response to external stimuli. For example, due to the photostability of the embedded metal tags,[105] spICP-MS analysis can track the size dependent photodegradation of PMMA NPs exposed 300 nm irradiation in the presence of H_2O_2. spICP-MS analysis showed that the overall NP concentration decreased systematically as a function of increasing irradiation time (Fig. 9). Additionally, visual inspection of the data collected at 0 hours and 6 hours demonstrates that there is a greater decrease in the number of NPs < 500 nm as compared to NPs > 900 nm, implicating a size dependent reactivity trend.

Among the most significant experimental advantages of our analytical approach is the ability to use unique metal tags for different NP types. This allows spICP-MS to simultaneously acquire data on the different metals present in mixtures, thereby enabling the PSD and PNC of different polymeric NPs to be determined in a single experiment. For example, in Fig. 10 we demonstrate concurrent detection and quantification of PVP tagged with Ta, PMMA tagged with Sn and PS tagged with Zr in the same solution *via* spICP-MS. In this example, the mass of the three polymer composites was varied to create a NP suspension where the observable particle number concentration of PS, PMMA, and PVP NPs was similar. It should be noted that this approach can also be extended to study NPs derived from the same polymer and subjected to different aging conditions (*e.g.*, one metal could be used to tag non-weathered PS NPs, while a different metal could be used to tag photochemically-weathered PS NPs). This can greatly reduce the experimental burden in studies designed to compare and contrast the behavior of NPs in different environments (*e.g.* soil transport and mesocosm studies), allowing a single experiment to yield data on up to as many as 4–5 different types of NPs while also ensuring that experimental conditions remain constant during data acquisition.

In addition to the aforementioned applications, the metal-tagged NPs could be utilized in studies designed to measure size-dependent NP uptake and toxicity in biological organisms since their surface properties are unchanged compared to those of the non-labelled NPs and the metal tags are not subject to leaching over the timescale of most biological uptake studies (see Fig. 5). For example, we have successfully used spICP-MS to quantify the uptake of heterogeneously sized PMMA NPs (tagged with Ta) into developing zebrafish larvae. The PSD of the NP taken up by the zebrafish and the original stock are compared in Fig. 11. Particle number in each size bin has been normalized by the total number measured (left axis, Fig. 11). Enhanced uptake of the smaller NPs is apparent, evidenced by the increasing ratio of NPs measured in the original stock used to dose the

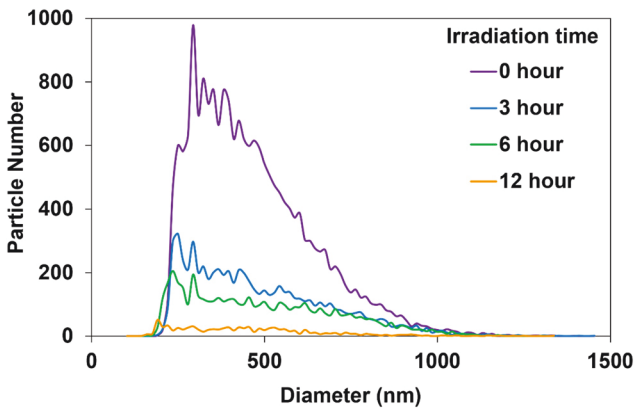

Fig. 9 Particle size distributions of a 1 w/w % Ta-PMMA NPs suspension over the course of 12 hours of accelerated photochemical weathering in the presence of 300 nm light and 200 mM hydrogen peroxide.

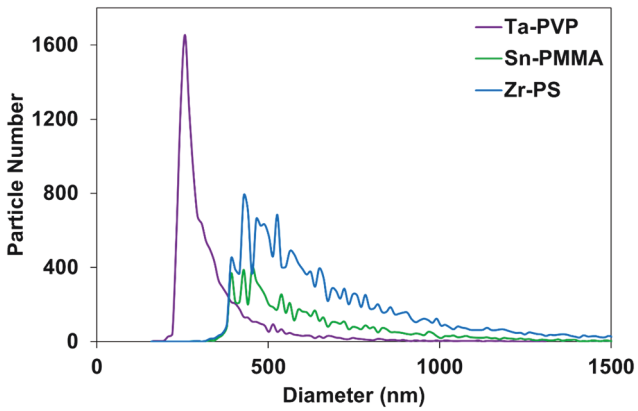

Fig. 10 Particle size distributions obtained for a sample containing a mixture of Ta-PVP, Sn-PMMA, and Zr-PS NPs suspended in water of equal amounts (by number density). All microplastics contained 1 w/w % metal loading.

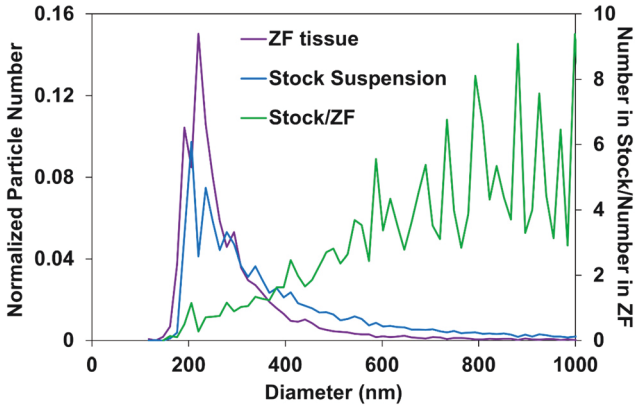

Fig. 11 Particle size distributions for PMMA nanoplastics containing 1 w/w % Ta uptaken by zebrafish larvae. Particle numbers are normalized to total number of measured particles. Further experimental details are described in the ESI.†

ZF to the NPs extracted from the ZF tissue, plotted as a function of NP size (right axis, Fig. 11). Application of metal-tagged NPs in biological uptake studies described here in could be expanded. For example, organic additives typically encountered in polymers (*e.g.* benzophenones) could also be introduced into the casting solution to create more chemically complex but realistic NPs.

There are, however, certain scenarios where the presence of the metal tags would likely preclude their application, for example, in NP biodegradation studies. It is also important to recognize that the method of NP preparation, particularly the use of sonication, may modify a polymer's average molecular weight[106–109] and therefore some of its physicochemical (*e.g.* mechanical) properties. Consequently, these altered polymer characteristics should be quantified in situations where NP behavior, or release potential is expected to be impacted such as in NP release as a result of wear or abrasion.

Conclusions

This study illustrates a new approach to synthesize labelled nanoplastics (NPs) for a wide range of polymer types, where the presence of uniformly distributed metal atoms enables counting and sizing of polydisperse NPs across a sub-micron size distribution by spICP-MS. This information enables us to quantify particle size distributions (PSDs) and particle number concentration (PNCs), even when the NPs are present at low μg L^{-1} concentrations. The elemental specificity of spICP-MS facilitates analysis in complex, multi-component matrices, which can contain background particles that would confuse other particle analysis methods (NTA, DLS). Moreover, the flexibility of the synthetic approach allows unique metal tags to be used for different NPs (*e.g.* Ta for PMMA, Sn for PVC) opening up the possibility to quantify the behavior of mixtures of polydisperse NPs under the same experimental conditions. In addition to the examples discussed, this new analytical approach could be applied to lab-based studies designed to study the behavior and release potential of NPs in other environmental matrices such as food, drinking water, packaging materials, and to assess potential routes of NP human health exposures (*e.g.* air-borne).

Ethical statement

All animal procedures were performed in accordance with the Guidelines for Care and Use of Laboratory Animals of Texas Tech University and approved by the Animal Ethics Committee under protocol number 2022-1281.

Conflicts of interest

There are no conflicts to declare.

Acknowledgements

This work was partially supported by the National Science Foundation (Grant No. 2003481). The authors would like to thank Patrick Eckhert for assistance with SEM imaging, as well as Nasim Ganji for assistance performing XPS measurements. μ-XRF scans were performed by the Minerals and Materials Characterization Laboratory at the Colorado School of Mines and at the National Renewable Energy Laboratory in Golden, CO.

References

1 R. Geyer, J. R. Jambeck and K. L. Law, *Sci. Adv.*, 2017, **3**, e1700782.
2 M. W. Ryberg, M. Z. Hauschild, F. Wang, S. Averous-Monnery and A. Laurent, *Resour., Conserv. Recycl.*, 2019, **151**, 104459.
3 D. M. Mitrano, P. Wick and B. Nowack, *Nat. Nanotechnol.*, 2021, **16**, 491–500.
4 J.-P. W. Desforges, M. Galbraith, N. Dangerfield and P. S. Ross, *Mar. Pollut. Bull.*, 2014, **79**, 94–99.
5 N. P. Ivleva, A. C. Wiesheu and R. Niessner, *Angew. Chem., Int. Ed.*, 2017, **56**, 1720–1739.
6 EFSA CONTAM Panel, *EFSA J.*, 2016, **14**, e04501.
7 K. Betts, *Environ. Sci. Technol.*, 2008, **42**, 8995.
8 N. B. Hartmann, T. Hüffer, R. C. Thompson, M. Hassellöv, A. Verschoor, A. E. Daugaard, S. Rist, T. Karlsson, N. Brennholt, M. Cole, M. P. Herrling, M. C. Hess, N. P. Ivleva, A. L. Lusher and M. Wagner, *Environ. Sci. Technol.*, 2019, **53**, 1039–1047.
9 F. Zhu, C. Zhu, C. Wang and C. Gu, *Bull. Environ. Contam. Toxicol.*, 2019, **102**, 741–749.
10 J. Li, D. Yang, L. Li, K. Jabeen and H. Shi, *Environ. Pollut.*, 2015, **207**, 190–195.
11 M. Cole, P. Lindeque, E. Fileman, C. Halsband, R. Goodhead, J. Moger and T. S. Galloway, *Environ. Sci. Technol.*, 2013, **47**, 6646–6655.
12 L. C. de Sá, M. Oliveira, F. Ribeiro, T. L. Rocha and M. N. Futter, *Sci. Total Environ.*, 2018, **645**, 1029–1039.
13 Y.-L. Wang, Y.-H. Lee, I.-J. Chiu, Y.-F. Lin and H.-W. Chiu, *Int. J. Mol. Sci.*, 2020, **21**, 1727.

14 M. F. M. Santana, F. T. Moreira and A. Turra, *Mar. Pollut. Bull.*, 2017, **121**, 154–159.
15 L. G. A. Barboza, A. Dick Vethaak, B. R. B. O. Lavorante, A.-K. Lundebye and L. Guilhermino, *Mar. Pollut. Bull.*, 2018, **133**, 336–348.
16 F. Ribeiro, D. M. Mitrano, C. Hacker, P. Cherek, K. Brigden, S. L. Kaserzon, K. V. Thomas and T. S. Galloway, *Environ. Sci. Technol.*, 2022, **56**, 16716–16725.
17 E.-L. Ng, E. Huerta Lwanga, S. M. Eldridge, P. Johnston, H.-W. Hu, V. Geissen and D. Chen, *Sci. Total Environ.*, 2018, **627**, 1377–1388.
18 S. Lambert and M. Wagner, *Chemosphere*, 2016, **145**, 265–268.
19 D. Sedlak, *Environ. Sci. Technol.*, 2017, **51**, 7747–7748.
20 S. Klein, E. Worch and T. P. Knepper, *Environ. Sci. Technol.*, 2015, **49**, 6070–6076.
21 S. Kühn, A. van Oyen, A. M. Booth, A. Meijboom and J. A. van Franeker, *Chemosphere*, 2018, **213**, 103–113.
22 A. Ter Halle and J. F. Ghiglione, *Environ. Sci. Technol.*, 2021, **55**, 14466–14469.
23 L. Sørensen, E. Rogers, D. Altin, I. Salaberria and A. M. Booth, *Environ. Pollut.*, 2020, **258**, 113844.
24 R. E. Engler, *Environ. Sci. Technol.*, 2012, **46**, 12302–12315.
25 K. Ashton, L. Holmes and A. Turner, *Mar. Pollut. Bull.*, 2010, **60**, 2050–2055.
26 M. Bittelli, G. S. Campbell and M. Flury, *Soil Sci. Soc. Am. J.*, 1999, **63**, 782–788.
27 Y. Li, E. Padoan and F. Ajmone-Marsan, *Ecotoxicol. Environ. Saf.*, 2021, **209**, 111806.
28 T. O. Sokmen, E. Sulukan, M. Turkoglu, A. Baran, M. Ozkaraca and S. B. Ceyhun, *Neurotoxicology*, 2020, **77**, 51–59.
29 M. Sun, R. Ding, Y. Ma, Q. Sun, X. Ren, Z. Sun and J. Duan, *Chemosphere*, 2021, **282**, 131124.
30 M. Torres-Ruiz, A. De la Vieja, M. de Alba Gonzalez, M. Esteban Lopez, A. Castano Calvo and A. I. Canas Portilla, *Sci. Total Environ.*, 2021, **797**, 149125.
31 H. Cheng, Z. Duan, Y. Wu, Y. Wang, H. Zhang, Y. Shi, H. Zhang, Y. Wei and H. Sun, *Environ. Int.*, 2022, **161**, 107128.
32 H. M. Dusza, E. A. Katrukha, S. M. Nijmeijer, A. Akhmanova, A. D. Vethaak, D. I. Walker and J. Legler, *Environ. Health Perspect.*, 2022, **130**, 97006.
33 R. Zhang, M. R. Silic, A. Schaber, O. Wasel, J. L. Freeman and M. S. Sepulveda, *Sci. Total Environ.*, 2020, **724**, 138065.
34 Z. Wang, T. Lin and W. Chen, *Sci. Total Environ.*, 2020, **700**, 134520.
35 M. Pivokonský, L. Pivokonská, K. Novotná, L. Čermáková and M. Klimtová, *Sci. Total Environ.*, 2020, **741**, 140236.
36 M. Pivokonsky, L. Cermakova, K. Novotna, P. Peer, T. Cajthaml and V. Janda, *Sci. Total Environ.*, 2018, **643**, 1644–1651.
37 T. Stanton, M. Johnson, P. Nathanail, R. L. Gomes, T. Needham and A. Burson, *Environ. Sci. Technol. Lett.*, 2019, **6**, 606–611.
38 G. Erni-Cassola, M. I. Gibson, R. C. Thompson and J. A. Christie-Oleza, *Environ. Sci. Technol.*, 2017, **51**, 13641–13648.
39 A. Barber, S. Kly, M. G. Moffitt, L. Rand and J. F. Ranville, *Environ. Sci.: Nano*, 2020, **7**, 514–524.
40 M. Mowla, S. Shakiba and S. M. Louie, *Chem. Commun.*, 2021, **57**, 12940–12943.
41 H. Fakour, S.-L. Lo, N. T. Yoashi, A. M. Massao, N. N. Lema, F. B. Mkhontfo, P. C. Jomalema, N. S. Jumanne, B. H. Mbuya, J. T. Mtweve and M. Imani, *Agriculture*, 2021, **11**, 330.
42 M. S. Bank, D. M. Mitrano, M. C. Rillig, C. Sze Ki Lin and Y. S. Ok, *Nat. Rev. Earth Environ.*, 2022, **3**, 736–737.
43 F. Caputo, R. Vogel, J. Savage, G. Vella, A. Law, G. Della Camera, G. Hannon, B. Peacock, D. Mehn, J. Ponti, O. Geiss, D. Aubert, A. Prina-Mello and L. Calzolai, *J. Colloid Interface Sci.*, 2021, **588**, 401–417.
44 A. Moraz and F. Breider, *Anal. Chem.*, 2021, **93**, 14976–14984.
45 F. Laborda, C. Trujillo and R. Lobinski, *Talanta*, 2021, **221**, 121486.
46 A. Prasad, J. R. Lead and M. Baalousha, *Sci. Total Environ.*, 2015, **537**, 479–486.
47 S. Kefer, O. Miesbauer and H.-C. Langowski, *Polymers*, 2021, **13**, 2881.
48 G. Balakrishnan, M. Déniel, T. Nicolai, C. Chassenieux and F. Lagarde, *Environ. Sci.: Nano*, 2019, **6**, 315–324.
49 A. G. Rodríguez-Hernández, J. A. Muñoz-Tabares, J. C. Aguilar-Guzmán and R. Vazquez-Duhalt, *Environ. Sci.: Nano*, 2019, **6**, 2031–2036.
50 V. C. F. Mosqueira, P. Legrand, H. Pinto-Alphandary, F. Puisieux and G. Barratt, *J. Pharm. Sci.*, 2000, **89**, 614–626.
51 N. Kalogerakis, K. Karkanorachaki, G. C. Kalogerakis, E. I. Triantafyllidi, A. D. Gotsis, P. Partsinevelos and F. Fava, *Front. Mar. Sci.*, 2017, **4**, 84.
52 Y. K. Song, S. H. Hong, M. Jang, G. M. Han, S. W. Jung and W. J. Shim, *Environ. Sci. Technol.*, 2017, **51**, 4368–4376.
53 E. von der Esch, M. Lanzinger, A. J. Kohles, C. Schwaferts, J. Weisser, T. Hofmann, K. Glas, M. Elsner and N. P. Ivleva, *Front. Chem.*, 2020, **8**, 169.
54 F. Blancho, M. Davranche, F. Fumagalli, G. Ceccone and J. Gigault, *Environ. Sci.: Nano*, 2021, **8**, 3211–3219.
55 L. Eitzen, S. Paul, U. Braun, K. Altmann, M. Jekel and A. S. Ruhl, *Environ. Res.*, 2019, **168**, 490–495.
56 A. Paul, L. Wander, R. Becker, C. Goedecke and U. Braun, *Environ. Sci. Pollut. Res.*, 2019, **26**, 7364–7374.
57 H. El Hadri, J. Gigault, B. Maxit, B. Grassl and S. Reynaud, *NanoImpact*, 2020, **17**, 100206.
58 J. Jiménez-Lamana, L. Marigliano, J. Allouche, B. Grassl, J. Szpunar and S. Reynaud, *Anal. Chem.*, 2020, **92**, 11664–11672.
59 Y. Lai, L. Dong, Q. Li, P. Li, Z. Hao, S. Yu and J. Liu, *Environ. Sci. Technol.*, 2021, **55**, 4783–4791.
60 L. Marigliano, B. Grassl, J. Szpunar, S. Reynaud and J. Jiménez-Lamana, *Molecules*, 2021, **26**, 7093.
61 A. E. P. del Real, D. M. Mitrano, H. Castillo-Michel, M. Wazne, J. Reyes-Herrera, E. Bortel, B. Hesse, J. Villanova and G. Sarret, *J. Hazard. Mater.*, 2022, **430**, 128356.
62 A. H. Tophinke, A. Joshi, U. Baier, R. Hufenus and D. M. Mitrano, *Environ. Pollut.*, 2022, **311**, 119933.
63 W. J. Shim, Y. K. Song, S. H. Hong and M. Jang, *Mar. Pollut. Bull.*, 2016, **113**, 469–476.

64 T. Maes, R. Jessop, N. Wellner, K. Haupt and A. G. Mayes, *Sci. Rep.*, 2017, **7**, 44501.
65 S. Piehl, A. Leibner, M. G. J. Löder, R. Dris, C. Bogner and C. Laforsch, *Sci. Rep.*, 2018, **8**, 17950.
66 M. Scheurer and M. Bigalke, *Environ. Sci. Technol.*, 2018, **52**, 3591–3598.
67 L. Yang, Y. L. Zhang, S. C. Kang, Z. Q. Wang and C. X. Wu, *Sci. Total Environ.*, 2021, **780**, 146546.
68 M. Moniruzzaman and K. I. Winey, *Macromolecules*, 2006, **39**, 5194–5205.
69 N. G. Sahoo, S. Rana, J. W. Cho, L. Li and S. H. Chan, *Prog. Polym. Sci.*, 2010, **35**, 837–867.
70 E. Dal Lago, E. Cagnin, C. Boaretti, M. Roso, A. Lorenzetti and M. Modesti, *Polymers*, 2019, **12**, 29.
71 K. Ke, Y. Wang, X.-Q. Liu, J. Cao, Y. Luo, W. Yang, B.-H. Xie and M.-B. Yang, *Composites, Part B*, 2012, **43**, 1425–1432.
72 J. C. Foster, I. Akar, M. C. Grocott, A. K. Pearce, R. T. Mathers and R. K. O'Reilly, *ACS Macro Lett.*, 2020, **9**, 1700–1707.
73 M. D. Montaño, H. R. Badiei, S. Bazargan and J. Ranville, *Environ. Sci.: Nano*, 2014, 338–346.
74 H. E. Pace, N. J. Rogers, C. Jarolimek, V. A. Coleman, C. P. Higgins and J. F. Ranville, *Anal. Chem.*, 2011, **83**, 9361–9369.
75 A. R. Deline, B. P. Frank, C. L. Smith, L. R. Sigmon, A. N. Wallace, M. J. Gallagher, D. G. Goodwin, D. P. Durkin and D. H. Fairbrother, *Chem. Rev.*, 2020, **120**, 11651–11697.
76 J. Yang, J. L. Bitter, B. A. Smith, D. H. Fairbrother and W. P. Ball, *Environ. Sci. Technol.*, 2013, **47**, 14034–14043.
77 B. Smith, J. Yang, J. Bitter, W. P. Ball and D. H. Fairbrother, *Environ. Sci. Technol.*, 2012, **46**, 12839–12847.
78 H.-H. Cho, K. Wepasnick, B. A. Smith, F. K. Bangash, D. H. Fairbrother and W. P. Ball, *Langmuir*, 2010, **26**, 967–981.
79 K. L. Chen, B. A. Smith, W. P. Ball and D. H. Fairbrother, *Environ. Chem.*, 2010, **7**, 10–27.
80 B. Smith, K. Wepasnick, K. E. Schrote, H.-H. Cho, W. P. Ball and D. H. Fairbrother, *Langmuir*, 2009, **25**, 9767–9776.
81 B. Smith, K. Wepasnick, K. E. Schrote, A. R. Bertele, W. P. Ball, C. O'Melia and D. H. Fairbrother, *Environ. Sci. Technol.*, 2009, **43**, 819–825.
82 H. Fairbrother, B. Smith, J. Wnuk, K. Wepasnick, W. P. Ball, H. Cho and F. K. Bangash, in *Environmental Nanomaterials*, ed. V. Grassian, John Wiley and Sons, New York, 2008, pp. 131–156.
83 H.-H. Cho, B. A. Smith, J. D. Wnuk, D. H. Fairbrother and W. P. Ball, *Environ. Sci. Technol.*, 2008, **42**, 2899–2905.
84 K.-Y. Law, *J. Phys. Chem. Lett.*, 2014, **5**, 686–688.
85 K.-Y. Law, *Pure Appl. Chem.*, 2015, **87**, 759–765.
86 M. Filella and J. Buffle, in *Colloids in the Aquatic Environment*, ed. T. F. Tadros and J. Gregory, Elsevier, Oxford, 1993, pp. 255–273, DOI: **10.1016/B978-1-85861-038-2.50021-8**.
87 S. G. Bevers, C. Smith, S. Brown, N. Malone, D. H. Fairbrother, A. J. Goodman and J. F. Ranville, *Environ. Sci.: Nano*, 2023, **10**, 3136–3148.
88 M. Cole, *Sci. Rep.*, 2016, **6**, 34519.
89 Z. Khodsiani, H. Mansuri and T. Mirian, *Powder Technol.*, 2013, **245**, 7–12.
90 N. Kumar and K. Biswas, *J. Mater. Res. Technol.*, 2019, **8**, 63–74.
91 C. J. McColley, J. A. Nason, B. J. Harper and S. L. Harper, *Microplast. Nanoplast.*, 2023, **3**, 20.
92 S. Prager and F. Long, *J. Am. Chem. Soc.*, 1951, **73**, 4072–4075.
93 J. F. N. Valderrama, K. Baek, F. J. Molina and I. J. Allan, *Environ. Sci.: Processes Impacts*, 2016, **18**, 87–94.
94 A. Reynier, P. Dole, S. Humbel and A. Feigenbaum, *J. Appl. Polym. Sci.*, 2001, **82**, 2422–2433.
95 C. Chen, L. Chen, Y. Yao, F. Artigas, Q. Huang and W. Zhang, *Environ. Sci. Technol.*, 2019, **53**, 10741–10752.
96 S. Bevers, C. Smith, S. Brown, N. Malone, D. H. Fairbrother and J. Ranville, *Manuscript submitted for publication*, 2023.
97 D. Metarapi, M. Šala, K. Vogel-Mikuš, V. S. Šelih and J. T. van Elteren, *Anal. Chem.*, 2019, **91**, 6200–6205.
98 M. Wang, L.-N. Zheng, B. Wang, H.-Q. Chen, Y.-L. Zhao, Z.-F. Chai, H. J. Reid, B. L. Sharp and W.-Y. Feng, *Anal. Chem.*, 2014, **86**, 10252–10256.
99 D. M. Mitrano, A. Beltzung, S. Frehland, M. Schmiedgruber, A. Cingolani and F. Schmidt, *Nat. Nanotechnol.*, 2019, **14**, 362–368.
100 N. J. Clark, F. R. Khan, C. Crowther, D. M. Mitrano and R. C. Thompson, *Sci. Total Environ.*, 2023, **854**, 158765.
101 N. J. Clark, F. R. Khan, D. M. Mitrano, D. Boyle and R. C. Thompson, *Environ. Int.*, 2022, **159**, 106994.
102 W. M. Heinze, D. M. Mitrano, E. Lahive, J. Koestel and G. Cornelis, *Environ. Sci. Technol.*, 2021, **55**, 16423–16433.
103 S. Frehland, R. Kaegi, R. Hufenus and D. M. Mitrano, *Water Res.*, 2020, **182**, 115860.
104 R. J. Rauschendorfer, K. M. Whitham, S. Summer, S. A. Patrick, A. E. Pierce, H. Sefi-Cyr, S. Tadjiki, M. D. Kraft, S. R. Emory, D. A. Rider and M. D. Montaño, *Front Toxicol.*, 2021, **3**, 752296.
105 K. D. Sullivan and V. Gugliada, *Mar. Pollut. Bull.*, 2018, **133**, 622–625.
106 K. S. Suslick and G. J. Price, *Annu. Rev. Mater. Sci.*, 1999, **29**, 295–326.
107 G. J. Price and P. F. Smith, *Polymer*, 1993, **34**, 4111–4117.
108 M. T. Taghizadeh and T. Asadpour, *Ultrason. Sonochem.*, 2009, **16**, 280–286.
109 M. T. Taghizadeh and A. Bahadori, *J. Polym. Res.*, 2009, **16**, 545–554.